

The Role of a Polariton Bath in the Emission Spectrum of an Open Nanocavity-Quantum Dot System

Nicolás Moure,¹ Herbert Vinck-Posada,² and Boris A. Rodríguez¹

¹*Instituto de Física, Universidad de Antioquia, Medellín, Colombia*

²*Departamento de Física, Universidad Nacional de Colombia, Bogotá, Colombia*

(Dated: December 3, 2024)

We investigate the effect of a polariton bath on the photoluminescence spectrum of the elementary excitations for a confined nanocavity-quantum dot (nC-QD) system. We modeled the nC-QD system as a two-level exciton in strong coupling with a single photonic cavity mode interacting with its environment. The non-hamiltonian processes induced by the environment are taken into account via a Born-Markov master equation which includes: gain and loss of excitons and photons into/out of the cavity, a dephasing mechanism produced by phonon scattering in the semiconductor lattice and gain and loss of polaritons due to the already mentioned polariton bath. A possible physical mechanism for the gain and loss of polaritons is discussed. Finally, to validate our model, we fit an experimental spectrum to extract the values of all parameters appearing in the master equation. Our results show that polariton pumping and loss rates are comparable to the other parameters and therefore we have a first evidence that the polariton bath we proposed has a significant role in the dynamics of a nC-QD system.

PACS numbers: 78.67.Hc, 42.55.Ah, 42.55.Sa

I. INTRODUCTION

Nanocavity quantum electrodynamics (nC-QED), the complex interplay between the methods of quantum optics and the specific nature of the solid state systems, has recently emerged as one of the most active and promising research fields^{1,2}. A single quantum emitter, a quantum dot (QD), coupled to one confined light mode in a photonic crystal, micropillar, or microdisk cavity is one of these nC-QED systems with more perspectives for device applications and fundamental physics such as: single photon sources³, quantum information processing⁴, strong coupling (SC)^{5–8}, and related phenomena such as non-classical light^{9,10}, strong optical nonlinearities^{11,12}, and control of cavity reflectivity¹³. More recently it has been reported controllable all-optical switching between laser pulses at the single photon level using a single QD and a photonic crystal cavity^{14,15}.

One of the most remarkable SC phenomena in nC-QED systems is the polariton physics^{1,16}. A polariton quasiparticle is an entangled state between semiconductor excitons and cavity mode photons that arise from the strong-coupling regime of the light-matter interaction. Despite more than twenty years of conducting theoretical and experimental research, the community do not agree yet with the main physics behind polariton phenomena^{17,18}. The large ground state occupation with spontaneous coherence build up can be understood in term of a polariton laser^{17,19–21} or as a non-equilibrium Bose-Einstein condensate^{18,22,23}.

Despite that SC is usually identified through their characteristic anticrossing in the photoluminescence emission spectrum⁵, detailed theoretical works has shown that this feature is not a unique fingerprint of SC⁷. The line splitting in the spectrum depends mainly on the interplay of dissipative and dephasing rates and therefore

when analyzing an experimental spectra a detailed modeling theory is needed. A surprising example of agreement between theory and experiment was done by Laucht *et al.* in Ref. 24. By fitting the theoretical spectrum with the experimental one, they extracted the whole set of parameters that characterize the interaction mechanisms between the nC-QD system and the environment: gain and loss of excitons and photons into/out of the cavity and a dephasing mechanism due to phonon scattering in the semiconductor lattice.

Motivated by the polariton laser experimental results¹⁹, recent theoretical works have proposed^{20,25} that some of the coherence properties of nC-QED systems can be understood in terms of an effective pumping of polaritons. In the former reference the authors have developed a finite system theory of multilevel QD with explicit electron-hole Coulomb interactions which is able to reproduce the experimental polariton laser threshold. In the latter work a Jaynes-Cummings approach was used, and it has shown how the incoherent polariton pumping is able to both sustain a large number of photons inside the cavity with Poisson-like statistics, and induce a separable exciton-photon state in the stationary limit. In addition, the authors also have shown that the polariton pumping is unable to modify the dynamical regimes of the system. However, in both works there is a lack of a comprehensive polariton bath theory.

In this work, we propose a master equation with a polariton bath, in addition to the already reported processes in the literature^{20,24–26}. Some of the advantages of this procedure are: the recognition of polariton loss as a relevant scattering process, the improvement in the definition of polaritonic transition operators as discussed in section II A, and the possibility to obtain a better agreement when fitting an experimental spectrum. In view of the high degree of complexity encountered in solid state

systems, this could represent another step towards a more comprehensive understanding of the nC-QD system.

The rest of the paper is organized as follows. In Sec. II, we describe the theoretical model used and write down the master equation with all the processes involved. We outline the Quantum Regression Theorem (QRT) equations, which permit us to calculate the emission spectrum beyond the linear regime. We also discuss a possible mechanism for polariton pumping and loss. In Sec. III, we show numerical results for the luminescence spectrum. We investigate the influence of our definition of the polariton transition operators and discuss the different approximations to the first excitation manifold found in the literature. In addition, we find the polariton pumping and loss rates by fitting a experimental spectrum. Concluding remarks are presented in Sec. IV. Finally, the appendices give some details about the density operator matrix elements, the QRT equations, and the approximations to the linear regime.

II. THEORETICAL MODEL

We are interested in a single quantum dot in interaction with one photonic mode of a semiconductor nC. For the purposes of our work we treat the QD as a two-level system (monoexcitonic regime). This model is customary in the literature and captures the main physics of the system²⁴⁻²⁷. Hence, an appropriate way of describing the intrinsic dynamics of the nC-QD system is by means of the Jaynes-Cummings hamiltonian²⁸

$$H_S = \frac{\hbar\omega_x}{2}\sigma_z + \hbar\omega_c a^\dagger a + \hbar g(\sigma_+ a + \sigma_- a^\dagger), \quad (1)$$

where σ_+ , σ_- and σ_z are pseudo-spin operators for the QD with ground state $|G\rangle$ and excited (exciton) state $|X\rangle$ separated by the exciton energy $\hbar\omega_x$. a^\dagger (a) is the creation (annihilation) operator of the nC mode with frequency ω_c , and g is the coupling strength between the photonic mode and the exciton. We are interested in the strong coupling regime. In this regime, the ‘‘dressed’’ states of the system

$$\begin{aligned} |n, +\rangle &= \cos\left(\frac{\phi_n}{2}\right)|Xn-1\rangle + \sin\left(\frac{\phi_n}{2}\right)|Gn\rangle, \\ |n, -\rangle &= -\sin\left(\frac{\phi_n}{2}\right)|Xn-1\rangle + \cos\left(\frac{\phi_n}{2}\right)|Gn\rangle, \\ \phi_n &= \tan^{-1}(2g\sqrt{n}/\Delta), \end{aligned} \quad (2)$$

represent quasi-particle states, where $|Gn\rangle$, $|Xn-1\rangle$ are the ‘‘bare’’ states of the nC-QD system and $\Delta = \omega_x - \omega_c$

is the detuning. These quasi-particles are called polaritons and their existence becomes evident by looking at the level anti-crossing in the emission spectra²⁹.

A. Master equation

In addition to loss and gain of excitons and photons, and a dephasing mechanism already considered in the literature^{24,26}, we propose a polariton bath that accounts for gain and loss of polaritons into and out of the system. Inspired in the work by Ciuti *et al.*³⁰, we suggest a possible mechanism by which polaritons could be pumped and loss. This mechanism, discussed below in section IIC, is modeled by the simple bath-system interaction hamiltonian

$$H_P^{SE} = \sum_{i,j,n} \sum_R \hbar\mu_{ijn}^R (b_{ijn,R}^\dagger P_{ij}^{(n)} + b_{ijn,R} P_{ij}^{(n)\dagger}), \quad (3)$$

where $b_{ijn,R}$, $b_{ijn,R}^\dagger$ are bosonic operators for the bath and $P_{ij}^{(n)}$, $P_{ij}^{(n)\dagger}$ are polaritonic transition operators defined by

$$\begin{aligned} P_{ij}^{(n)} &= \sqrt{n+1}|n,j\rangle\langle n+1,i| & (\Lambda_{n+1} \rightarrow \Lambda_n); \\ P_{ij}^{(n)\dagger} &= \sqrt{n+1}|n+1,i\rangle\langle n,j| & (\Lambda_n \rightarrow \Lambda_{n+1}), \end{aligned} \quad (4)$$

where $i, j \in \{+, -\}$, $n = 0, 1, \dots, \infty$, and $\Lambda_n = \{|Gn\rangle, |Xn-1\rangle\}$ is the n th excitation manifold. H_P^{SE} takes into account situations in which a boson from the reservoir is absorbed ($b_{ijn,R}$) causing a polaritonic transition $|n, j\rangle \rightarrow |n+1, i\rangle$ ($P_{ij}^{(n)\dagger}$) along with the opposite processes. Both channels are controlled by a coupling constant μ_{ijn}^R . In previous works^{20,25}, similar transition operators to those on (4) were defined. However, we have introduced the factor $\sqrt{n+1}$ to account for the growth of polariton gain and loss rates with excitation number as can be expected if we look at their photonic analogs (see Eqs. (A1)). This factor is responsible for the non-linear behavior of the polariton loss and pumping processes with the excitation manifold.

Following the Born-Markov formalism^{31,32} and using an environment-system interaction hamiltonian containing H_P^{SE} among with those hamiltonians responsible for the above mentioned processes, we arrive to a master equation for the density operator of the nC-QD system:

$$\begin{aligned}
\frac{d\rho}{dt} = & -\frac{i}{\hbar}[H_S, \rho] + \frac{\gamma_\phi}{2}(\sigma_z \rho \sigma_z - \rho) + \frac{P_a}{2}(2a^\dagger \rho a - a a^\dagger \rho - \rho a a^\dagger) + \frac{\gamma_a}{2}(2a \rho a^\dagger - a^\dagger a \rho - \rho a^\dagger a) \\
& + \frac{P_\sigma}{2}(2\sigma_+ \rho \sigma_- - \sigma_- \sigma_+ \rho - \rho \sigma_- \sigma_+) + \frac{\gamma_\sigma}{2}(2\sigma_- \rho \sigma_+ - \sigma_+ \sigma_- \rho - \rho \sigma_+ \sigma_-) \\
& + \frac{P_p}{2} \sum_{ijn} \left(2P_{ij}^{(n)\dagger} \rho P_{ij}^{(n)} - P_{ij}^{(n)} P_{ij}^{(n)\dagger} \rho - \rho P_{ij}^{(n)} P_{ij}^{(n)\dagger} \right) + \frac{\gamma_p}{2} \sum_{ijn} \left(2P_{ij}^{(n)} \rho P_{ij}^{(n)\dagger} - P_{ij}^{(n)\dagger} P_{ij}^{(n)} \rho - \rho P_{ij}^{(n)\dagger} P_{ij}^{(n)} \right).
\end{aligned} \tag{5}$$

In this master equation, γ_ϕ is a pure dephasing rate induced by constant scattering processes between the QD and the semiconductor lattice phonons, P_a represents the photonic pumping rate caused by the emission of decoupled QD's present in the nC, γ_a is the cavity loss rate (coherent emission), P_σ is the rate at which excitons are incoherently pumped by optical or electrical excitation, γ_σ is the exciton decay rate (spontaneous emission), and finally P_p and γ_p are respectively, the rates at which polaritons are created and lost (see Fig. 1). The incoherent pumping and loss processes cause incoherent transitions among “bare” and “dressed” states of two consecutive excitation manifolds²⁵.

Eq. (5) can be transformed in an infinite set of linear differential equations for the density operator matrix elements on the direct product basis $\{|Gn\rangle, |Xn\rangle\}$. When the system is initially in its ground state, there is a closed set of equations for the nC-QD populations ($\rho_{Gn, Gn}, \rho_{Xn, Xn}$) and coherences between levels in the same excitation manifold Λ_{n+1} ($\rho_{Gn+1, Xn}$). This set of linear equations is found in Appendix A (Eqs. A1). It is useful for practical computational purposes and it

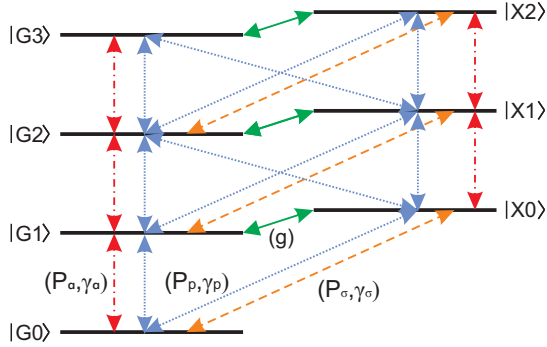


FIG. 1. (Color online) Transitions between “bare” energy levels induced by the hamiltonian and non-hamiltonian processes. Green continuous arrows represent transitions due to the nC-QD interaction. Red dot-dashed arrows show photon gain and loss transitions. Orange dashed arrows depict transitions caused by the exciton pumping and loss processes. Finally, the blue dotted arrows correspond to the polariton bath induced transitions. The dephasing mechanism is not displayed since it does not cause transitions between energy levels, it only modifies the non-diagonal density matrix elements.

provides a better understanding of the effect caused by system-environment interaction processes. From Eqs. (A1) it becomes clear that the overall effect of these processes is to cause transitions between excitation manifolds and to reduce coherence in the system.

B. Emission spectrum

When dealing with experimental samples of the nC-QD system, the emission spectrum is one of the most accessible observables. Assuming that the principal cause of light emission of the system is due to cavity leakage, the spectral function in the stationary state is given by

$$S(\omega) \propto \lim_{t \rightarrow \infty} \text{Re} \int_0^\infty d\tau e^{-(\gamma+i\omega)\tau} \langle a^\dagger(t+\tau)a(t) \rangle, \tag{6}$$

which is the Fourier transform of the cavity field correlation function $g^{(1)}(t, \tau) = \langle a^\dagger(t+\tau)a(t) \rangle$ weighted by the factor $e^{-\gamma\tau}$ to account for additional broadening of the spectral lines due to the finite resolution of the detectors²⁴.

Our calculation of the correlation function closely resembles the one by Tejedor and co-workers²⁶. First, we write operator a^\dagger as

$$a^\dagger = \sum_n \sqrt{n+1} (a_{Gn}^\dagger + a_{Xn}^\dagger), \tag{7}$$

where $a_{Gn}^\dagger = |Gn+1\rangle\langle Gn|$ and $a_{Xn}^\dagger = |Xn+1\rangle\langle Xn|$. Using the master equation (Eq. (5)) it is possible to find a closed set of linear differential equations including the expectation values of a_{Gn}^\dagger and a_{Xn}^\dagger (see Appendix B, Eqs. (B1)). According to the Quantum Regression Theorem (QRT), time evolution for expectation values $\langle a_{Gn}^\dagger(t+\tau)a(t) \rangle$, $\langle a_{Xn}^\dagger(t+\tau)a(t) \rangle$, $\langle \sigma_n^\dagger(t+\tau)a(t) \rangle$, and $\langle \varsigma_n(t+\tau)a(t) \rangle$, is also governed by Eqs. (B1) with initial conditions

$$\begin{aligned}
\langle a_{Gn}^\dagger(t)a(t) \rangle &= \sqrt{n+1} \rho_{Gn+1, Gn+1}(t), \\
\langle a_{Xn}^\dagger(t)a(t) \rangle &= \sqrt{n+1} \rho_{Xn+1, Xn+1}(t), \\
\langle \sigma_n^\dagger(t)a(t) \rangle &= \sqrt{n+1} \rho_{Gn+1, Xn}(t), \\
\langle \varsigma_n(t)a(t) \rangle &= \sqrt{n} \rho_{Xn, Gn+1}(t),
\end{aligned} \tag{8}$$

where t stands for the time in which the system has reached the stationary state, and operators $\sigma_n^\dagger =$

$|Xn\rangle\langle Gn|$ and $\varsigma_n = |Gn+1\rangle\langle Xn-1|$ were introduced in order to keep the linear system closed. After solving Eqs. (B1) with initial conditions given in Eqs. (8), we can compute the first correlation function as

$$g^{(1)}(t, \tau) = \sum_n \sqrt{n+1} \left(\langle a_{Gn}^\dagger(t+\tau)a(t) \rangle + \langle a_{Xn}^\dagger(t+\tau)a(t) \rangle \right). \quad (9)$$

Now, with the knowledge of $g^{(1)}(t, \tau)$, the emission spectrum is obtained via Eq. (6). The main advantage of the previous approach is that we can calculate the emission spectrum beyond the first excitation manifold without doing any further approximations.

C. Polariton pumping and loss mechanism

Here we discuss the physical origin of a possible mechanism for polariton pumping and loss. In the experimental sample we are interested in, the nC-QD system is embedded in a p - i - n junction with a potential difference applied to both its ends to control the exciton frequency ω_x via the confined stark effect³³. In an analogous way to the theory developed by Ciuti *et al.*³⁰ for a quantum well, polariton states can be efficiently created in a nC-QD system by injecting electrons in the electron states of the QD. Using a second quantization formalism, and taking into account the quantum dot internal structure with a multi-mode nC, we can have a more complete hamiltonian for the nC-QD system similar to the one proposed by Ciuti:

$$\begin{aligned} H_{QD} = & \sum_i \hbar\omega_{e,i} e_i^\dagger e_i + \sum_j \hbar\omega_{h,j}(k) h_j^\dagger h_j \\ & + \sum_q \hbar\omega_{c,q} a_q^\dagger a_q \\ & + \sum_{i,i',q} \hbar\chi_q a_q h_i^\dagger e_i^\dagger + \sum_{i,i',q} \hbar\chi_q a_q^\dagger e_i h_{i'}. \end{aligned} \quad (10)$$

Here, e_i^\dagger (e_i) is the creation (annihilation) operator for an electron in state $|e_i\rangle$ with energy $\hbar\omega_{e,i}$. Equivalently, h_j^\dagger (h_j) is the creation (annihilation) operator for a ‘‘hole’’ in state $|h_j\rangle$ with an energy of $\hbar\omega_{h,j}$. Sums over q run over the cavity modes. The coupling constant χ_q controls both interaction channels present in the hamiltonian. The first channel represents processes in which a photon is absorbed (a_q), resulting in the creation of an electron-hole pair ($h_i^\dagger e_i^\dagger$). The second channel involves opposite processes.

The polariton formation described by the hamiltonian in Eq. (10) is essentially different from the one caused by the Jaynes-Cummings hamiltonian intrinsic dynamics, so we can consider it as an external pumping (or loss) in our effective dynamic theory.

III. NUMERICAL RESULTS

A. Polariton pumping and emission spectrum

In this section we show the effect in the emission spectrum caused by the excitation manifold dependent factor in the polariton ladder operators definition (Eqs. (4)). In previous works^{20,25}, this factor was not introduced which then leaves the effective polariton pumping and loss rates independent from the excitation number. From Eqs. (A1), it can be seen that effective photonic rates grow with the photon number n , a behavior that we reproduce for polariton rates by introducing the factor $\sqrt{n+1}$ in Eqs. (4).

In Fig. 2, we show emission spectra calculated with and without the factor $\sqrt{n+1}$ in the ladder operators definition. For low polariton rates ($P_p = 10^{-3}$ meV/ \hbar), the difference between both spectral lines is almost negligible. This is expected since for low pumping rates, the population for excitation manifolds higher than Λ_1 are much less than one, making the dependence with n almost irrelevant. However, for higher pumping rates ($P_p = 10^{-2}$ meV/ \hbar), both spectral functions appreciably differ from each other. In fact, the interior peaks have a greater intensity if the spectrum is calculated with ladder operators given by Eqs. (4). Again, this is expected since for excitation number dependent polariton pumping, the second excitation manifold populations are higher and the interior peaks correspond to transitions $|2, \pm\rangle \rightarrow |1, \pm\rangle$. Additionally, there is a minor increment in the line widths, since decoherence effects are larger

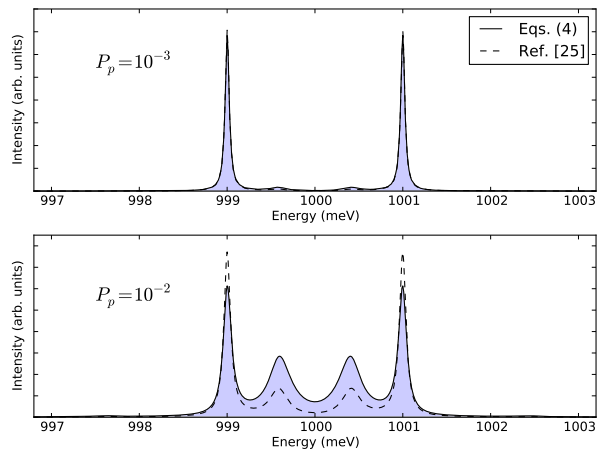


FIG. 2. Emission spectra using two definitions for the polariton ladder operators for $P_p = 10^{-3}$ meV/ \hbar (top) and $P_p = 10^{-2}$ meV/ \hbar (bottom). Continuous shadowed lines represent spectral functions calculated with Eqs. (4), whereas dashed lines correspond to emission spectra calculated without the factor $\sqrt{n+1}$ as is used in Ref. [25]. The other parameters in the master equation were fixed to $\omega_c = 1000$ meV, $g = 1$ meV/ \hbar , $\hbar\gamma_a = 0.1$ meV/ \hbar , and the other ones to zero $\Delta = P_a = P_\sigma = \gamma_\sigma = \gamma_\phi = 0$.

when the factor $\sqrt{n+1}$ is introduced (see Eqs. (A1)).

B. Approximations to the emission spectrum

The importance of computing the emission spectrum using the exact dynamics of the first correlation function governed by Eqs. (B1) is developed in this section. For this purpose, we fix the polariton pumping and loss rates to zero throughout this section.

There are at least two ways of finding an approximation to the emission spectrum. The first one is to approximate the first correlation function up to the first excitation manifold³⁴. This leaves us with the following set of differential equations

$$\begin{aligned} \frac{d}{d\tau} \langle a^\dagger(\tau) \rangle &= (i\omega_c - \Gamma_1) \langle a^\dagger(\tau) \rangle + ig \langle \sigma_+(\tau) \rangle \\ \frac{d}{d\tau} \langle \sigma_+(\tau) \rangle &= ig \langle a^\dagger(\tau) \rangle + (i\omega_x - \Gamma'_1) \langle \sigma_+(\tau) \rangle, \end{aligned} \quad (11)$$

where $\Gamma_1 = 3P_a/2 + \gamma_a/2 + P_\sigma$ and $\Gamma'_1 = P_a + P_\sigma/2 + \gamma_\sigma/2 + \gamma_\phi$. Then, the first correlation function $g^{(1)}(t, \tau)$ can be found by using the Quantum Regression Theorem. The second way is due to Finley and co-workers^{24,35}, and it combines the first approximation with the exact solution as we show on Appendix C. Again, the problem becomes two-dimensional and the spectrum is computed via

$$\begin{aligned} \frac{d}{d\tau} \langle a^\dagger(\tau) \rangle &= (i\omega_c - \Gamma_2) \langle a^\dagger(\tau) \rangle + ig \langle \sigma_+(\tau) \rangle \\ \frac{d}{d\tau} \langle \sigma_+(\tau) \rangle &= ig \langle a^\dagger(\tau) \rangle + (i\omega_x - \Gamma'_2) \langle \sigma_+(\tau) \rangle, \end{aligned} \quad (12)$$

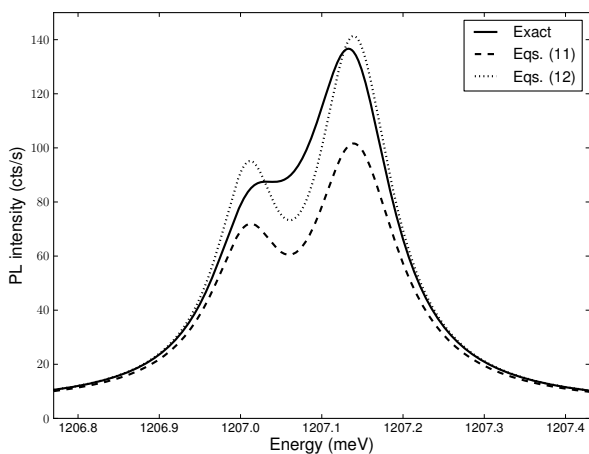


FIG. 3. Emission spectra calculated with three different methods for the parameters reported by Finley and co-workers²⁴ ($g = 59 \mu\text{eV}/\hbar$, $P_a = 4.5 \mu\text{eV}/\hbar$, $P_\sigma = 0.5 \mu\text{eV}/\hbar$, $\gamma_a = 68.0 \mu\text{eV}/\hbar$, $\gamma_\sigma = 0.2 \mu\text{eV}/\hbar$, and $\gamma_\phi = 19.9 \mu\text{eV}/\hbar$). The continuous line is the PL spectrum computed with the exact expansion (Eqs. (B1)) up to Λ_{25} . Dashed and dotted lines correspond to the spectrum calculated with Eqs. (11) and Eqs. (12), respectively.

where $\Gamma_2 = \gamma_a/2 - P_a/2$ and $\Gamma'_2 = P_\sigma/2 + \gamma_\sigma/2 + \gamma_\phi$.

Even though both approximations are good for low pumping rates, they are unable to reproduce the exact spectrum for typical parameters controlling the dynamics of the nC-QD system in real experimental setups as displayed in Fig. 3.

C. Theoretically fitting an experimental emission spectrum

To validate our model of the polariton bath, we followed a similar procedure to the one developed by Finley and co-workers^{24,35}. By fitting one of their experimental spectrums²⁴ we were able to find values for the coupling constant g and the gain and loss rates involved in our master equation (Eq. (5)). Both the detuning and the cavity mode were experimentally determined by Finley's Group so they are not included in the fitting process and remain fixed at $\Delta = -50 \mu\text{eV}/\hbar$ and $\omega_c = 1207.1 \text{ meV}/\hbar$. We also use their estimated value of the broadening parameter appearing in Eq. (6), $\gamma = 30 \mu\text{eV}/\hbar^2$.

Based on the results of the previous section, when fitting an experimental emission spectrum it is of great importance to compute $g^{(1)}(t, \tau)$ using the exact expansion (Eq. (9)) since for some range of parameters the two approximations mentioned above are not able to reproduce the actual spectral lines. As a consequence, we don't have an analytical expression for $S(\omega)$ so we can't use a regular minimum square algorithm to fit the spectrum. To overcome this obstacle we used a Simulated Annealing (SA) algorithm³⁶ defining the cost function as the sum of square differences between the experimental and theoretical spectral lines

$$\mathcal{S}^2 = \sum_i (S(\omega_i) - S_{exp}(\omega_i))^2, \quad (13)$$

where $S_{exp}(\omega_i)$ is the experimental PL intensity at frequency ω_i , and the index i runs over the available data. SA has proven to be a fairly good tool to optimize functions in high parametric spaces making it the best choice for our purposes.

The best fit (displayed in Fig. 4) was obtained for $g = 67.93 \mu\text{eV}/\hbar$, $P_p = 0.02 \mu\text{eV}/\hbar$, $P_a = 2.27 \mu\text{eV}/\hbar$, $P_\sigma = 2.32 \mu\text{eV}/\hbar$, $\gamma_p = 8.96 \mu\text{eV}/\hbar$, $\gamma_a = 31.82 \mu\text{eV}/\hbar$, $\gamma_\sigma = 10.12 \mu\text{eV}/\hbar$, and $\gamma_\phi = 7.40 \mu\text{eV}/\hbar$. These values show that polariton pumping and loss rates are comparable to the other parameters, indicating that the polariton bath we proposed has a significant role in the dynamics of the nC-QD system. A conclusion that can be drawn given the quality of our fit.

Additionally, to strengthen our result we use a control experimental spectrum from Ref. 24 with $\Delta = +50 \mu\text{eV}/\hbar$. The experimental data along the theoretical curve computed with the fitting parameters, are illustrated in Fig. 4. This control spectrum shows that the parameters obtained are also good to describe the characteristic asymmetric double peak features near resonance.

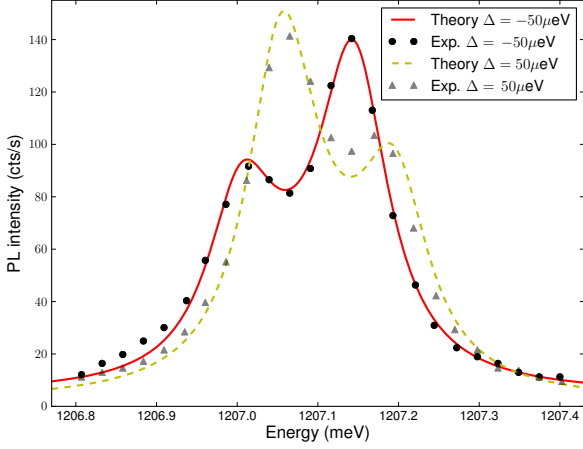


FIG. 4. (color online) Theoretical fit and control spectra. The continuous red line shows the theoretical PL spectrum fitting the experimental data (black dots) at $\Delta = -50 \mu\text{eV}/\hbar$. The dashed yellow line is the control spectrum and the grey triangles are the experimental intensities at $\Delta = +50 \mu\text{eV}/\hbar$. The cost function is $\mathcal{S} = 12.6 \text{ cts/s}$ in the first case, and $\mathcal{S} = 29.8 \text{ cts/s}$ in the second one. The fundamental mode frequency is fixed at $\omega_c = 1207.1 \text{ meV}/\hbar$.

IV. CONCLUSIONS

To summarize, we have presented a model for a polariton bath interacting with a nC-QD system. By theo-

retically fitting a photoluminescence spectrum, we were able to show that our model agrees with the experiment for non-zero values of the polariton pumping and loss rates. These values have the same order-of-magnitude of the rest master equation parameters, showing that at least from a phenomenological point of view the polariton gain and loss processes are feasible in real nC-QED systems. Additionally, we have shown the importance of computing the PL spectrum with the exact dynamics of the first correlation function. The two approximations we have discussed, fail to give an accurate description of the nC-QD system in real experimental conditions.

ACKNOWLEDGMENTS

We gratefully acknowledge partial financial support from Dirección de Investigación - Sede Bogotá, Universidad Nacional de Colombia (DIB-UNAL), and CODI at Universidad de Antioquia. The authors thank Dr. Juliana Restrepo, Prof. Paulo S. S. Guimarães and Prof. Karen M. Fonseca Romero for useful discussions. B.A.R. acknowledge the support of Departamento de Física, Universidade Federal de Minas Gerais for a short term visit.

Appendix A: Density operator matrix elements equations

Denoting matrix elements by $\rho_{Im,Jn} = \langle Im|\rho|Jn\rangle$, with $I, J \in \{G, X\}$, and using Eq. (5), is straightforward to show that

$$\begin{aligned} \frac{d}{dt}\rho_{Gn,Gn} &= n(P_a + P_p)\rho_{Gn-1,Gn-1} + nP_p\rho_{Xn-2,Xn-2} \\ &\quad - \{(n+1)P_a + n\gamma_a + P_\sigma + 2(n+1)P_p + (2 - \delta_{n1})n\gamma_p\}\rho_{Gn,Gn} + ig\sqrt{n}\rho_{Gn,Xn-1} \\ &\quad - ig\sqrt{n}\rho_{Xn-1,Gn} + (n+1)(\gamma_a + \gamma_p)\rho_{Gn+1,Gn+1} + \{\gamma_\sigma + (n+1)\gamma_p\}\rho_{Xn,Xn}, \end{aligned} \quad (\text{A1a})$$

$$\begin{aligned} \frac{d}{dt}\rho_{Xn,Xn} &= \{P_\sigma + (n+1)P_p\}\rho_{Gn,Gn} + \{nP_a + (n+1)P_p\}\rho_{Xn-1,Xn-1} \\ &\quad - \{(n+1)P_a + n\gamma_a + \gamma_\sigma + 2(n+2)P_p + (2 - \delta_{n0})(n+1)\gamma_p\}\rho_{Xn,Xn} - ig\sqrt{n+1}\rho_{Gn+1,Xn} \\ &\quad + ig\sqrt{n+1}\rho_{Xn,Gn+1} + (n+2)\gamma_p\rho_{Gn+2,Gn+2} + \{(n+1)\gamma_a + (n+2)\gamma_p\}\rho_{Xn+1,Xn+1}, \end{aligned} \quad (\text{A1b})$$

$$\begin{aligned} \frac{d}{dt}\rho_{Gn+1,Xn} &= \sqrt{n(n+1)}P_a\rho_{Gn,Xn-1} + \sqrt{(n+1)(n+2)}\gamma_a\rho_{Gn+2,Xn+1} \\ &\quad + \left\{ i\Delta - (2n+3)\frac{P_a}{2} - (2n+1)\frac{\gamma_a}{2} - \frac{P_\sigma}{2} - \frac{\gamma_\sigma}{2} - \gamma_\phi - 2(n+2)P_p - (2 - \delta_{n0})(n+1)\gamma_p \right\} \rho_{Gn+1,Xn} \\ &\quad + ig\sqrt{n+1}\rho_{Gn+1,Gn+1} - ig\sqrt{n+1}\rho_{Xn,Xn}, \end{aligned} \quad (\text{A1c})$$

Since $\rho_{Xn, Gn+1} = \rho_{Gn+1, Xn}^*$, the equation governing time evolution for $\rho_{Xn, Gn+1}$ is found by taking the complex conjugate of Eq. (A1c). As mentioned above, this linear set of differential equations is quite useful to find the time evolution of the density operator ρ .

Appendix B: QRT equations

Expectation values for a_{Gn}^\dagger , a_{Xn}^\dagger , σ_n^\dagger , ς_n can be written in terms of density operator matrix elements using the master equation (Eq. 5). Their time evolution can be easily found to be

$$\begin{aligned} \frac{d}{d\tau} \langle a_{Gn}^\dagger(\tau) \rangle = & \left\{ i\omega_c - \frac{P_a}{2}(2n+3) - \frac{\gamma_a}{2}(2n+1) - P_\sigma - P_p(2n+3) - \frac{\gamma_p}{2}[(2-\delta_{n1})n + (2-\delta_{n0})(n+1)] \right\} \langle a_{Gn}^\dagger(\tau) \rangle \\ & + P_a \sqrt{n(n+1)} \langle a_{Gn-1}^\dagger(\tau) \rangle - ig\sqrt{n} \langle \varsigma_n(\tau) \rangle + \gamma_a \sqrt{(n+1)(n+2)} \langle a_{Gn+1}^\dagger(\tau) \rangle + \gamma_\sigma \langle a_{Xn}^\dagger(\tau) \rangle + ig\sqrt{n+1} \langle \sigma_n^\dagger(\tau) \rangle; \end{aligned} \quad (\text{B1a})$$

$$\begin{aligned} \frac{d}{d\tau} \langle a_{Xn}^\dagger(\tau) \rangle = & \left\{ i\omega_c - \frac{P_a}{2}(2n+3) - \frac{\gamma_a}{2}(2n+1) - \gamma_\sigma - P_p(2n+5) - \frac{\gamma_p}{2}[(2-\delta_{n0})(n+1) + 2(n+2)] \right\} \langle a_{Xn}^\dagger(\tau) \rangle \\ & + P_a \sqrt{n(n+1)} \langle a_{Xn-1}^\dagger(\tau) \rangle + ig\sqrt{n+2} \langle \varsigma_{n+1}(\tau) \rangle + \gamma_a \sqrt{(n+1)(n+2)} \langle a_{Xn+1}^\dagger(\tau) \rangle + P_\sigma \langle a_{Gn}^\dagger(\tau) \rangle - ig\sqrt{n+1} \langle \sigma_{n+1}^\dagger(\tau) \rangle; \end{aligned} \quad (\text{B1b})$$

$$\begin{aligned} \frac{d}{d\tau} \langle \sigma_n^\dagger(\tau) \rangle = & \left\{ i\omega_x - P_a(n+1) - \gamma_a n - \frac{P_\sigma}{2} - \frac{\gamma_\sigma}{2} - \gamma_\phi - P_p(2n+3) - \frac{\gamma_p}{2}[(2-\delta_{n0})(n+1) + (2-\delta_{n1})n] \right\} \langle \sigma_n^\dagger(\tau) \rangle \\ & + P_a n \langle \sigma_{n-1}^\dagger(\tau) \rangle + \gamma_a (n+1) \langle \sigma_{n+1}^\dagger(\tau) \rangle + ig\sqrt{n+1} \langle a_{Gn}^\dagger(\tau) \rangle - ig\sqrt{n} \langle a_{Xn-1}^\dagger(\tau) \rangle; \end{aligned} \quad (\text{B1c})$$

$$\begin{aligned} \frac{d}{d\tau} \langle \varsigma_n(\tau) \rangle = & \left\{ i(2\omega_c - \omega_x) - P_a(n+1) - \gamma_a n - \frac{P_\sigma}{2} - \frac{\gamma_\sigma}{2} - \gamma_\phi - P_p(2n+3) - \frac{\gamma_p}{2}[(2-\delta_{n0})(n+1) + (2-\delta_{n1})n] \right\} \langle \varsigma_n(\tau) \rangle \\ & + P_a \sqrt{n^2-1} \langle \varsigma_{n-1}(\tau) \rangle + \gamma_a \sqrt{n(n+2)} \langle \varsigma_{n+1}(\tau) \rangle + ig\sqrt{n+1} \langle a_{Xn-1}^\dagger(\tau) \rangle - ig\sqrt{n} \langle a_{Gn}^\dagger(\tau) \rangle. \end{aligned} \quad (\text{B1d})$$

From Eqs. (B1), it becomes clear that the position of spectral peaks solely depends on g , ω_x , ω_c . This means that dissipation and pumping rates only modify their intensity and width. This is expected since population dynamics and decoherence properties are ruled by these rates.

Appendix C: Approximations to the emission spectrum: Derivations

Both approximations to the emission spectrum discussed in section IIIB can be derived from Eqs. (B1), which describe the exact dynamics of the first correlation function $g^{(1)}(t, \tau)$. The first approximation is straight forward. Up to Λ_1 , we have $\langle a^\dagger \rangle \approx \langle a_{G0}^\dagger \rangle$ and $\langle \sigma_+ \rangle \approx \langle \sigma_0^\dagger \rangle$ so that other expectation values in Eqs. (B1) become zero, leaving the two-dimensional system in Eqs. (11). To derive the second approximation we need to find the exact time derivatives of $\langle a^\dagger \rangle$ and $\langle \sigma_+ \rangle$. From Eqs. (B1), summing over all values of n and simplifying, we find

$$\begin{aligned} \frac{d}{d\tau} \langle a^\dagger(\tau) \rangle = & \left\{ i\omega_c + \frac{P_a}{2} - \frac{\gamma_a}{2} \right\} \times \\ & \sum_{n=0}^{\infty} \sqrt{n+1} (\langle a_{Gn}^\dagger(\tau) \rangle + \langle a_{Xn}^\dagger(\tau) \rangle) \\ & + ig \sum_{n=0}^{\infty} \langle \sigma_n^\dagger(\tau) \rangle, \end{aligned} \quad (\text{C1})$$

$$\begin{aligned} \frac{d}{d\tau} \langle \sigma_+(\tau) \rangle = & \left\{ i\omega_x - \frac{P_\sigma}{2} - \frac{\gamma_\sigma}{2} - \gamma_\phi \right\} \sum_{n=0}^{\infty} \langle \sigma_n^\dagger(\tau) \rangle \\ & - ig \sum_{n=0}^{\infty} \sqrt{n+1} (\langle a_{Xn}^\dagger(\tau) \rangle - \langle a_{Gn}^\dagger(\tau) \rangle), \end{aligned} \quad (\text{C2})$$

It is worth noting that this pair of equations are exact and cannot be found by doing the first excitation manifold approximation. From Eq. (7) and since $\sigma_+ = \sum_n \sigma_n^\dagger$, we have that Eq. (C1) is precisely the first line in Eqs. (12). However, to obtain the second line, it is necessary to approximate the second sum in Eq. (C2) to Λ_1 , i.e.,

$$\begin{aligned} \sum_{n=0}^{\infty} \sqrt{n+1} (\langle a_{Xn}^\dagger(\tau) \rangle - \langle a_{Gn}^\dagger(\tau) \rangle) \approx & -\langle a_{G0}^\dagger \rangle, \\ \approx & -\langle a^\dagger \rangle. \end{aligned} \quad (\text{C3})$$

This may be objectionable, since to find Eq. (C2) we had to sum over all excitation manifolds and now we are approximating the last sum to Λ_1 .

-
- ¹ A. Kavokin, J. Baumberg, G. Malpuech, and F. Laussy, *Microcavities*, Series on Semiconductor Science and Technology (Oxford University Press, 2011).
- ² E. Reboul, *Microcavity Quantum Electrodynamics* (VDM Verlag, 2010).
- ³ C. Santori, D. Fattal, J. Vučković, G. S. Solomon, and Y. Yamamoto, *Nature* **419**, 594 (2002).
- ⁴ A. Faraon, A. Majumdar, D. Englund, E. Kim, M. Bajcsy, and J. Vučković, *New Journal of Physics* **13**, 055025 (2011).
- ⁵ J. P. Reithmaier, G. Sek, A. Löffler, C. Hofmann, S. Kuhn, S. Reitzenstein, L. V. Keldysh, V. D. Kulakovskii, T. L. Reinecke, and A. Forchel, *Nature* **432**, 197 (2004).
- ⁶ T. Yoshie, A. Scherer, J. Hendrickson, G. Khitrova, H. M. Gibbs, G. Rupper, C. Ell, O. B. Shchekin, and D. G. Deppe, *Nature* **432**, 200 (2004).
- ⁷ F. P. Laussy, E. del Valle, and C. Tejedor, *Phys. Rev. Lett.* **101**, 083601 (2008).
- ⁸ P. C. Cárdenas, N. Quesada, H. Vinck-Posada, and B. A. Rodríguez, *Journal of Physics: Condensed Matter* **23**, 265304 (2011).
- ⁹ D. Press, S. Götzinger, S. Reitzenstein, C. Hofmann, A. Löffler, M. Kamp, A. Forchel, and Y. Yamamoto, *Phys. Rev. Lett.* **98**, 117402 (2007).
- ¹⁰ A. Faraon, I. Fushman, D. Englund, N. Stoltz, P. Petroff, and J. Vuckovic, *Nature Physics* **4**, 859 (2008).
- ¹¹ K. Srinivasan and O. Painter, *Nature* **450**, 862 (2007).
- ¹² I. Fushman, D. Englund, A. Faraon, N. Stoltz, P. Petroff, and J. Vukovi, *Science* **320**, 769 (2008).
- ¹³ D. Englund, A. Faraon, I. Fushman, N. Stoltz, P. Petroff, and J. Vukovi, *Nature* **450**, 857 (2007).
- ¹⁴ D. Englund, A. Majumdar, M. Bajcsy, A. Faraon, P. Petroff, and Vuckovic, *Phys. Rev. Lett.* **108**, 093604 (2012).
- ¹⁵ R. Bose, D. Sridharan, H. Kim, G. S. Solomon, and E. Waks, *Phys. Rev. Lett.* **108**, 227402 (2012).
- ¹⁶ H. M. Gibbs, G. Khitrova, and S. W. Koch, *Nature Photonics* **5**, 275 (2011).
- ¹⁷ L. V. Butov and A. V. Kavokin, *Nature Photonics* **6**, 2 (2012).
- ¹⁸ B. Deveaud-Plédran, *Nature Photonics* **6**, 205 (2012).
- ¹⁹ D. Bajoni, P. Senellart, E. Wertz, I. Sagnes, A. Miard, A. Lemaitre, and J. Bloch, *Phys. Rev. Lett.* **100**, 047401 (2008).
- ²⁰ C. A. Vera, H. Vinck-Posada, and A. González, *Phys. Rev. B* **80**, 125302 (2009).
- ²¹ D. G. Suárez-Forero, G. Cipagauta, H. Vinck-Posada, K. M. Fonseca-Romero, and B. A. Rodríguez, eprint arXiv:1205.2719 (2012), arXiv:1205.2719 [cond-mat.mes-hall].
- ²² J. Kasprzak, M. Richard, S. Kundermann, A. Baas, P. Jeambrun, J. M. J. Keeling, F. M. Marchetti, M. H. Szymanska, R. Andre, J. L. Staehli, V. Savona, P. B. Littlewood, B. Deveaud, and L. S. Dang, *Nature* **443**, 409 (2006).
- ²³ H. Deng, H. Haug, and Y. Yamamoto, *Rev. Mod. Phys.* **82**, 1489 (2010).
- ²⁴ A. Laucht, N. Hauke, J. M. Villas-Bôas, F. Hofbauer, G. Böhm, M. Kaniber, and J. J. Finley, *Phys. Rev. Lett.* **103**, 087405 (2009).
- ²⁵ N. Quesada, H. Vinck-Posada, and B. A. Rodríguez, *Journal of Physics: Condensed Matter* **23**, 025301 (2011).
- ²⁶ J. I. Perea, D. Porrás, and C. Tejedor, *Phys. Rev. B* **70**, 115304 (2004).
- ²⁷ E. del Valle, F. P. Laussy, and C. Tejedor, *Phys. Rev. B* **79**, 235326 (2009).
- ²⁸ E. T. Jaynes and F. W. Cummings, *Proc. IEEE* **51**, 89 (1963).
- ²⁹ H. Deng, D. Press, S. Götzinger, G. S. Solomon, R. Hey, K. H. Ploog, and Y. Yamamoto, *Phys. Rev. Lett.* **97**, 146402 (2006).
- ³⁰ S. De Liberato and C. Ciuti, *Phys. Rev. B* **79**, 075317 (2009).
- ³¹ H.-P. Breuer and F. Petruccione, *The Theory of Open Quantum Systems* (Oxford University Press, 2002).
- ³² M. Schlosshauer, *Decoherence and the Quantum-to-Classical Transition* (Springer-Verlag, 2007).
- ³³ A. Laucht, F. Hofbauer, N. Hauke, J. Angele, S. Stobbe, M. Kaniber, G. Böhm, P. Lodahl, M.-C. Amann, and J. J. Finley, *New Journal of Physics* **11**, 023034 (2009).
- ³⁴ H. J. Carmichael, R. J. Brecha, M. G. Raizen, H. J. Kimble, and P. R. Rice, *Phys. Rev. A* **40**, 5516 (1989).
- ³⁵ A. Laucht, J. M. Villas-Bôas, S. Stobbe, N. Hauke, F. Hofbauer, G. Böhm, P. Lodahl, M.-C. Amann, M. Kaniber, and J. J. Finley, *Phys. Rev. B* **82**, 075305 (2010).
- ³⁶ W. Press, *Numerical Recipes: The Art of Scientific Computing* (Cambridge University Press, 2007).